Volume 17 (1998), number 1 pp. 29–54 COMPUTER GRAPHICS forum

Adaptive Supersampling in Object Space Using Pyramidal Rays

Jon Genetti†, Dan Gordon‡ and Glen Williams§

Abstract

We introduce a new approach to three important problems in ray tracing: antialiasing, distributed light sources, and fuzzy reflections of lights and other surfaces. For antialiasing, our approach combines the quality of supersampling with the advantages of adaptive supersampling. In adaptive supersampling, the decision to partition a ray is taken in image-space*, which means that small or thin objects may be missed entirely. This is particularly problematic in animation, where the intensity of such objects may appear to vary. Our approach is based on considering pyramidal rays (pyrays) formed by the viewpoint and the pixel. We test the proximity of a pyray to the boundary of an object, and if it is close (or marginal), the pyray splits into 4 sub-pyrays; this continues recursively with each marginal sub-pyray until the estimated change in pixel intensity is sufficiently small.*

The same idea also solves the problem of soft shadows from distributed light sources, which can be calculated to any required precision. Our approach also enables a method of defocusing *reflected pyrays, thereby producing realistic fuzzy reflections of light sources and other objects. An interesting byproduct of our method is a substantial speedup over regular supersampling even when* all *pixels are supersampled. Our algorithm was implemented on polygonal and circular objects, and produced images comparable in quality to stochastic sampling, but with greatly reduced run times.*

Keywords: Computer graphics; picture/image generation; three-dimensional graphics and realism; antialiasing; distributed light sources; fuzzy reflections; penumbra; object-space; ray tracing; stochastic sampling; adaptive; supersampling.

1. Introduction

Ray tracing has been one of the foremost methods for displaying complex images[1]. Its chief advantages are its ability to handle many different shading models, complex reflections, refractions, and many different object types. Some disadvantages we will address are slowness, aliasing problems and difficulties with distributed light sources (which are problematic for other techniques as well). Another problem is that ray tracing by itself does not produce a complete solution to the rendering equation[2, 3], but even so, it is used by some of the more complex techniques as an essential step[3, 4, 5].

Most approaches to antialiasing can be considered *image-space*, since it is essentially the image-space that determines if and where extra rays have to be cast. We informally call an approach *object-space* if decisions regarding extra rays are based on information obtained during the ray-object intersections. Whitted's method[6] calls for a sufficiently large bounding volume to surround small objects, so that rays intersecting it will be subdivided. This component of the algorithm is object-space dependent, though the rest is not. Beam tracing[7] is an object-space approach because all calculations on beams are done in object-space. More recently, there have appeared two new object-space approaches to antialiasing[8, 9].

Another difficult problem for ray tracing (and other techniques) is distributed light sources. The standard

† San Diego Supercomputer Center, P.O. Box 85608, San Diego, CA 92186-9784, USA

‡ Dept. of Computer Science, University of Haifa, Haifa 31905, Israel

§ Dept. of Computer Science, Texas A&M University, College Station, TX 77843-3112, USA

way to calculate shadows is by tracing a shadow ray to a point light source, but this does not extend easily to distributed light sources. Beam tracing can handle such sources, but it is restricted to polygonal environments. Cone tracing can handle spherical light sources, but these are different from distributed sources because they illuminate with the same intensity in all directions. Furthermore, as shall be explained later, shadow calculations with cone tracing can be inaccurate. Stochastic sampling[10] handles the problem in a very time-consuming manner by distributing *many* rays across the light source. Other approaches (discussed in Section 2) are also time-consuming.

Specular reflections from point light sources are handled by standard ray tracing in an ideal manner—at least from the algorithmic, if not the physical, point of view. However, distributed light sources are problematic. Furthermore, real-life scenes contain fuzzy reflections not only of light sources, but of other reflected objects, and the problem is to introduce fuzziness into such reflections. This fuzziness varies with the angle of incidence and the surface characteristics, and current approaches are very time-consuming.

In this paper, a new *object-space* approach to the problems of antialiasing, distributed light sources and fuzzy reflections is presented. We call this method ASOS (adaptive supersampling in object-space). The general flavor is that of Whitted's adaptive supersampling, with the difference being that decisions to subdivide are taken in *object-space*. Pyramidal rays are traced through the scene, and when such a ray is close to an object boundary, it is subdivided. Ray subdivision is also used for antialiasing shadows and texture maps. This approach offers the quality of supersampling with the advantages of adaptive supersampling (only areas of high frequency information are supersampled). Furthermore, as will be explained in Subsection 2.3, our method eliminates a problem that is inherent with Whitted's object-space component of adaptive supersampling.

Our technique also solves the problem of penumbrae from distributed light sources, producing accurate shadows. All intensity and shadow computations can be carried out to any user-prescribed degree of accuracy. This is extremely useful for animation, where small or thin objects must not only be detected, but their area should be estimated correctly to prevent flashing or pulsating. The same holds for small or thin shadows, holes, or gaps between objects. Also, our method yields a simple solution to the problem of fuzzy reflections of lights and other objects, with the amount of fuzziness depending on the incidence angle and wavelength. As an added byproduct, our data structures and algorithms provide a substantial speedup over regular supersampling even when *all* pixels are supersampled, so our approach can also be viewed as a useful acceleration technique.

To place our work in proper historical perspective, a few notes are in order. In[6], Whitted writes: "...A better method, currently being investigated, considers volumes defined by each set of four corner rays and applies a containment test for each volume." In[11], Amanatides writes in a footnote that Whitted abandoned the pyramidal ray approach due to the complex calculations that are involved. This paper may be viewed as an implementation of Whitted's idea, carried out with adaptive supersampling in object space as a solution to the problem of complex calculations, as well as to the problem of fuzzy reflections. We also use circular cones as an aid in detecting the proximity of a pyramidal ray to an object. Solving the problems of antialiasing, distributed light sources, etc., involves computations that require integration over finite solid angles. This is done typically by point sampling, but the convergence is slow. Our method may be viewed as a more effective adaptive integration technique.

Comparisons between rendering techniques are usually done on the basis of image quality and speed. ASOS is a new ray tracing technique that produces images comparable in quality with stochastic sampling (without refractions), but at times that are usually smaller by an order of magnitude (when compared to the standard implementation). We do not give a complete solution to the rendering equation[2, 3, 4, 5], nor do we deal with special acceleration techniques for very complex scenes, such as[12, 13]. However, other approaches that use ray tracing as an essential step could take advantage of our technique. A preliminary version of this research has appeared in[14], and many of the technical details can be found in[15, 16].

The rest of the paper is organized as follows: Section 2 presents an overview of some of the current methods, together with their main advantages and disadvantages. Section 3 describes our technique of adaptive supersampling in object-space. Section 4 describes how shadows from point light sources are antialiased and how accurate penumbrae from distributed light sources may be calculated. Section 5 explains our defocusing method for producing fuzzy (specular) reflections of lights and other surfaces. Section 6 discusses some implementation and efficiency issues. Section 7 presents some results obtained with this technique and compares them with stochastic sampling. Section 8 concludes with a discussion and a summary of further applications.

2. Background

There have been three main approaches to the aliasing problem. One is to generate a fixed number of extra

rays for each pixel. Examples of this are simple averaging and supersampling. A logical extension to the first approach is to *adaptively* generate more rays for each pixel until some criterion is met. Examples are adaptive supersampling[6] and stochastic sampling[17, 18, 19]. See[1, 20, 21] for comprehensive discussions of these topics. The last approach has been to extend the definition of a ray—either to a different object or to allow more than one ray to be traced at a time. Several examples of this are discussed below.

2.1. Averaging

The simplest way to correct for aliasing is a simple averaging, such as replacing each pixel value by a (weighted) average of its neighbours. Another approach is to cast rays at the corners of pixels and to take their average as the pixel values. The disadvantage of these methods is that small objects may be missed, and some jagged effects may still be seen. These methods are collectively referred to as post processing by using a low pass filter.

2.2. Supersampling

Supersampling is done by sampling the image at a higher resolution than the screen, typically 4 to 16 rays per pixel. This method yields good results, but at a very high price in computation time. In most parts of an image, just one ray per pixel (corner) is sufficient.

2.3. Adaptive Supersampling

This method, due to Whitted[6], consists of casting rays through the corners of a pixel. If the 4 values do not differ from each other by much, their average is used for the pixel. If they do differ, more rays are cast—through the center of the pixel and the centers of the pixel edges. This subdivision continues as needed until some preset limit on the number of subdivisions is reached.

This method has a potential problem with small objects, which may escape undetected. Whitted corrects this by surrounding each small object with a bounding sphere sufficiently large so that if the object projection intersects a pixel, then at least one of the 4 rays will intersect the sphere. When this happens, the pixel is subdivided as before. We refer to this component of the algorithm as being done in *object-space*, because the decision to subdivide is based on information in object-space.

Some problems inherent to this approach have no solution: one cannot detect and antialias small or thin shadows (when the shadow is horizontal or vertical), and small or thin holes or gaps between objects. Even if they are detected and a single image looks good, animation sequences are problematic. Another problem is that rays reflected off a curved surface may still miss the bounding sphere of a small object.

2.4. Stochastic Sampling

Yellot[22] noticed that using an irregular sampling pattern caused some sampling effects to be converted to a particular form of noise which appears uniform to a human observer. Cook, Porter and Carpenter[17] introduced the technique of distributed ray tracing. Their method consists of evaluating pixel values by stochastically supersampling[10] and distributing the rays across those domains that need to be made "fuzzy". This method can be used not only to correct for antialiasing, but also to produce other effects such as penumbrae, blurred reflections, motion blur, and simulation of depth-of-field effects. On the pixel size that he worked with, Cook reached the conclusion that some 16 rays per pixel produced a reasonable noise. With stochastic sampling, aliasing artifacts are replaced by noise, to produce a pleasing picture while requiring less sampling than would be necessary with a regular sampling pattern. Lee et al.[23] analysed the relationship between the number of samples per pixel and the quality of the estimate obtained, and presented an optimized algorithm for antialiasing, penumbrae, fuzzy reflections, wavelength sampling, and more.

2.5. Adaptive Stochastic Sampling

Dippé and Wold[18] studied the use of noise-reducing filters to improve the quality of the image at a given sampling rate, and applied this technique to antialiasing ray traced images. The filter width is controlled adaptively, but this is based on image-space data. Mitchell[19] used adaptive supersampling based on results obtained in image-space. He used Poisson-disk sampling, and introduced a scanline algorithm to generate the sampling pattern in an efficient manner. Painter and Sloan[24] also used adaptive supersampling based on results in image-space, but their procedure started from above the pixel level. They used both a confidence interval test (to determine when supersampling should be stopped), and a coverage condition to ensure that all objects larger than a pixel are sampled.

2.6. Beam Tracing

In beam tracing[7], an initial beam, formed by the viewpoint and the view plane, is traced through the image. When this beam intersects a surface, the exact portion of the beam that continues past a polygon (if any) is calculated using a clipping algorithm such as the Weiler-Atherton algorithm[25]. The resulting beam continues to the next object, while the intersection is reflected as another beam. This method is completely accurate but it

is limited to polygonal scenes. The original paper discusses extensions to directional light sources, but not distributed ones. However, these can be handled in principle by tracing a beam from a surface point towards such a source.

2.7. Cone Tracing

In cone tracing[11], a ray is replaced by a cone surrounding the viewpoint and the pixel. When a cone intersects the boundary of an object, the *fraction* of the occluded cone is calculated, and the cone is then continued past the object with a suitably reduced intensity. Although this method produces reasonable antialiasing, soft shadows, and fuzzy reflections, it is not accurate, because it does not account for the fact that a cone may be blocked in various orientations. For example, suppose a cone is 50% blocked by one surface and then 50% blocked by a further surface. In reality, the two surfaces may be directly behind one another (totaling only 50% blockage), or they may be occluding the entire cone; cone tracing does not distinguish between these cases.

Another major distinction between cone tracing and our approach to soft shadows is that in cone tracing, the light source is considered as a sphere with equal intensity towards all directions (unless shadowed), while our technique also handles distributed light sources such as arbitrarily-shaped lighted polygons whose intensity varies with the angle of incidence, just as in radiosity.

2.8. Covers

Covers[8] is an extension of Whitted's bounding spheres. Objects are assumed to be surrounded by some covers of a sufficient thickness to ensure that they are intersected by a ray from at least one pixel. Thus, when a ray intersects a cover, it is in proximity to the boundary of an object. In this case, the pixel's intensity is taken as a weighted average of the two intensities. This is an object-space technique which solves some problems, but creates others. For example, covers must be quite large if one is to account for reflected rays, particularly for rays reflected off a curved surface. As in cone-tracing, this method cannot distinguish between different orientations of objects in a ray's path. Another potential problem with this method occurs with thin or small objects: since the weights are based only on the distance to the closest edge, such an object will not accurately contribute its weight to the pixel value. Shadows are handled by considering their edges on the surface, hence the method is inherently limited to point light sources.

2.9. Ray Bound Tracing

In ray bound tracing[9], a ray bound surrounding several similar rays is used to detect the proximity of the rays to the boundary of an object. When this happens, the pixel is supersampled at some predetermined value (16 samples were used in their sample images). The drawback of a predetermined supersampling rate is that many samples must be used to capture very small or thin objects. Compared to adaptive approaches, the number of extra samples can be very high. The method is limited to point light sources and it is not clear if it can be extended to distributed sources.

2.10. Pencil Tracing

Shinya et al.[26] define a pencil as a bundle of rays which are close to a central "axial" ray. The rays in a pencil are called "paraxial", and each can be represented in the pencil coordinate system as a 4-dimensional vector. Their approach is based on the premise that at an object surface, each paraxial ray undergoes a transformation which can be approximated by a linear transformation, represented by a 4×4 "system" matrix. This approach does not work for pencils which intersect object boundaries or edges, where regular ray tracing is used. The paper uses pencil tracing to create images containing curved surfaces, perfect reflections, refractions and point light sources. There doesn't seem to be a direct use of this method for distributed light sources. As for fuzzy reflections, it is far from clear that such reflections can be properly approximated by a linear transformation. The paper deals only with point light sources and parallel rays (produced by a point source at infinity).

2.11. Global Illumination Methods

Several papers present solution methods for the global illumination problem[27, 28, 2, 3, 4, 5]. They handle the problem of antialiasing, penumbrae from distributed light sources and fuzzy reflections. They are very time consuming, and some of them involve two phases: one is view-independent (such as radiosity and its extensions), and the other is view-dependent. Those methods that involve a view-dependent stage use various flavors of ray tracing, some of which may be speeded up by our approach.

2.12. Coverage Masks

Fiume[29] presents an efficient method of antialiasing by approximating the coverage of a pixel. The method uses coverage masks and convolution tables to achieve fast area sampling. However, the technique is non-adaptive: it uses a fixed subdivision of a pixel, even in regions of low frequency.

3. Adaptive Supersampling in Object-space

Our method can be viewed as an extension of Whitted's adaptive supersampling approach carried out in *object-*

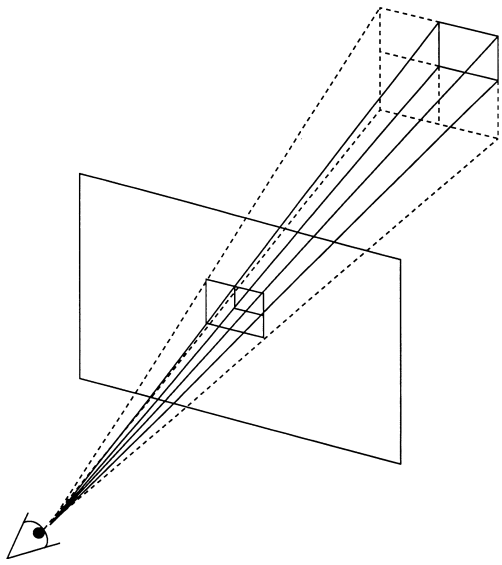

Figure 1: *A pyramidal ray subdivided into 4.*

space. The mathematical ray (semi-infinite line) is viewed as if surrounded by a pyramidal ray formed by the viewpoint and the original pixel. This pyramidal ray is mathematically also a cone, but to distinguish it from a circular cone we call it a *pyray*.

In standard ray tracing, a ray either meets an object or it doesn't. When a pyray and an object are involved there are three possible outcomes: the pyray completely intersects the object, or it completely misses it, or it is *marginal* (i.e., part of the pyray meets the object and part of it misses it). When a pyray is marginal with respect to an object, we split it up into 4 sub-pyrays, and the procedure is repeated for each sub-pyray. Figure 1 shows a pyramidal ray subdivided into 4 sub-pyrays. This process continues to any desired accuracy, giving the user an easily controlled trade-off between image quality and processing time. Finally, when a pyray (or sub-pyray) has to return a value from the surface, it is sampled by its center, or, in some cases by a point jittered from the center.

As an aid in detecting whether a pyray is marginal, we surround it by a circular cone and detect intersections using the cone. We consider the pyray to be marginal if the enclosing *cone* intersects the object. This will cause some pyrays to be split even if no object boundary intersects it, but there is no loss of accuracy involved. The slight increase in the number of marginal pyrays is more than offset by the simplicity (and time-saving) of testing the proximity of a circular cone to an object. Note that we are not doing cone tracing because only points that are strictly inside the pyray are used as sample points; the cone is merely used as an aid to deciding marginality.

We use the term ray in its classical sense to refer to the line going from the viewpoint through the center of the pixel. We sometimes also refer to this ray as the *axis* of the pyray. When a pyray splits into four, the central (mathematical) rays of the sub-pyrays are called *subrays* of the original ray. For convenience, the original pyray is called a 0-ray, its sub-pyrays are called 1-rays, and so on. The decision on whether a sub-pyray should be subdivided is done by estimating an upper bound on the intensity change that could be produced by subdividing. If the estimated change is less than some user-supplied value ε, no subdivisions are done. The parameter ε controls the tradeoff between image quality and processing time. It allows us to guarantee the capture of arbitrarily small (or narrow) objects simply by making ε sufficiently small.

At the lowest level of subdivision, we no longer consider the sub-pyrays, but just the regular subrays, as in ordinary ray tracing. At this level, we can also jitter the subrays, so that any aliasing artifacts that are left are replaced by noise which seems featureless. This can be done because at that level we no longer need the symmetry required for subdivision.

Our technique can be easily extended to support a filter that is larger than a pixel: we can simply surround each pixel with a larger square and cast the pyray through that square instead of the pixel.

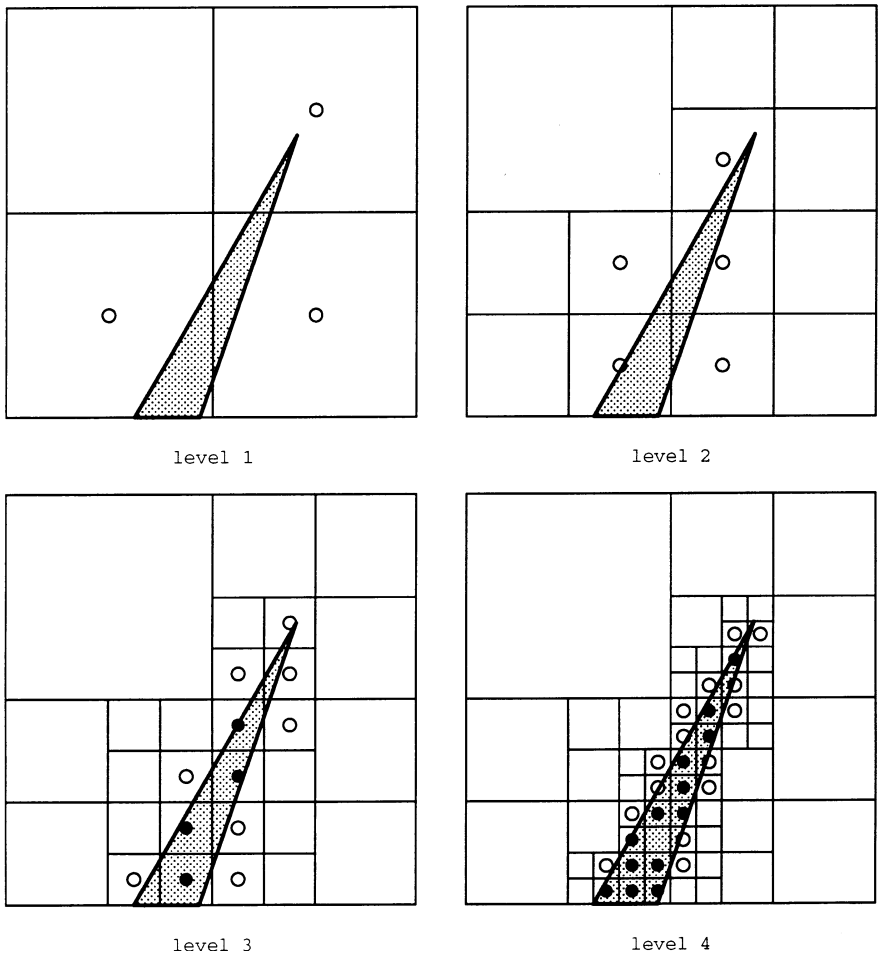

Figure 2: *Intersection of thin object and pyray, showing adaptive subdivision at levels 1 to 4.*

3.1. Subdivision Stopping Criterion

In this section we derive a simple mathematical upper bound on the change that would be produced in pixel intensity if marginal sub-pyrays are subdivided. This bound is then used in our stopping criterion.

Let us assume that a 0-ray is marginal with respect to an object. The algorithm then does a subdivision, resulting in 4 1-rays. In general, assume that we have divided the marginal rays up to a level of K, so we now have to determine which (if any) of the K-rays have to be subdivided. Clearly, only the marginal K-rays are candidates for subdivision. Let M be the total number of marginal K-rays, IN the number of marginal K-rays whose axis hits the object, and OUT=M−IN. Now denote L=max(IN, OUT), and we assume for the sake of discussion that L=IN.

There are two alternatives in our scheme: to subdivide all the M marginal rays, or not to subdivide any of them. We can calculate the maximum possible change in pixel intensity that would be produced by subdividing. If the L K-rays that are *in* are subdivided, it is possible that the (K+1)-subrays of each of them will all be *out* (e.g., in the case of a thin object). This could be balanced by some of the M−L *out* K-rays spawning some (K+1)-subrays that are *in*, but in the worst case, this will not happen. The area of every K-ray is $1/2^{2K}$, so the maximum area that could be affected by the change is $L/2^{2K}$. If we assume intensities in the range of 0 to 1, then we see that the maximum change in the pixel intensity is again just $L/2^{2K}$. This leads us to the following decision criterion:

If $L/2^{2K} \leq \varepsilon$ then stop subdividing (the marginal rays).

The above comparison can be expressed in the form $L \leq 2^{2K}\varepsilon$. When we go from K to K+1, $2^{2K}\varepsilon$ increases by 4. Note that we should have some maximum allow-

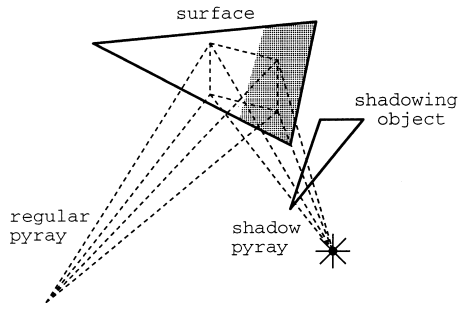

Figure 3: *Generating accurate shadows from a point light source by casting a shadow pyray.*

able depth of subdivision so that the program does not continue subdividing in case of pathological situations. We can construct an object so that the center of the initial 0-ray will be *in*, then all the 1-subrays will be *out*, then all the 2-subrays will be *in* again, and so on. We denote the maximum level by MAX with MAX=4 sufficient for most practical purposes, since this allows up to 256 4-rays or a 16×16 supersample.

Figure 2 shows an example with $\varepsilon=1/16$, so $2^{2K}\varepsilon = 2^{2K-4}$.

K=1 M=3, IN=0, OUT=3 so L=3. $2^{2K-4} = 1/4 < \mathrm{L}$ so we subdivide the marginal 1-rays.

K=2 M=5, IN=0, OUT=5, so L=5. $2^{2K-4} = 1 < \mathrm{L}$ so we subdivide the marginal 2-rays.

K=3 M=12, IN=4, OUT=8, so L=8. $2^{2K-4} = 4 < \mathrm{L}$ so we subdivide the marginal 3-rays

K=4 M=28, IN=13, OUT=15, so L=15. Now $2^{2K-4} = 16 > \mathrm{L}$ so we stop at this stage.

It is interesting to note that in this example, the difference between the approximated area of the object (14 4-rays) and the actual area is just 0.63% of the entire area covered by the original pixel.

Although our stopping criterion may appear similar to the well-known *adaptive tree-depth control* of ray tracing[1], it is in reality very different. In adaptive tree-depth control, a decision with regard to every node of the tree is made based only on the estimated contribution of that single node. However, it is possible that several nodes will each be determined as making a small contribution, but collectively, their contribution could be significant. In contrast, our stopping criterion considers the *total* change in pixel intensity that would be produced by *all* the candidates for subdivision. Hence, our results are guaranteed to be accurate to within the user-supplied tolerance ε.

3.2. Textured Surfaces

Textured surfaces present a different problem: we may need to sample a patch even if it is not marginal, otherwise we may get aliasing effects. Our solution to this is simply to force a pyray (or sub-pyray) that is entirely inside a textured surface to subdivide up to some user-prescribed level. This gives us yet another user-controlled parameter that provides a trade-off between image quality and processing time.

We define the TR (texture resolution) as the resolution to which a non-marginal pyray subdivides when it hits a textured-mapped surface. For example, TR=3 means that each such pyray samples the texture map 9 times by subdividing into a 3×3 mesh. Within each small square, we sample the texture by a point jittered from the center, in order to correct any aliasing that is left.

4. Shadows

In this section we discuss the handling of shadows from various sources, including penumbrae and the problem of antialiasing. In all the following, when we consider pyrays intersecting a surface, we assume that it intersects it completely—otherwise the pyray would have split and the pyray under consideration is actually a sub-pyray.

4.1. Shadows from Point Light Sources

In regular ray tracing, when a ray hits a surface, a shadow ray is traced towards the point light source, and depending on whether the shadow ray hits an object, it is determined whether the surface point is in shadow or not. The problem with this approach is that shadows can become aliased. Our approach provides a simple solution to this problem: when a pyray intersects a surface, it creates a surface patch with four corners. We construct a *shadow pyray* by taking the light (which is a point) as the source and having the four lines connecting the light to the patch's corners as the shadow pyray's corners. The axis of the pyray is drawn from the light to the point of intersection of the surface and the original pyray's axis. Figure 3 illustrates this construction.

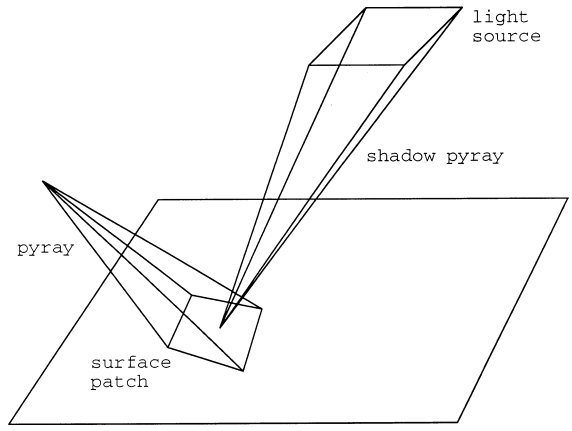

Figure 4: *Shadow pyray from a surface point to a distributed light source.*

We now handle the shadow pyray similarly to a regular pyray: it either completely misses all objects on the way to the patch (in which case the patch is completely lit), or it is completely obstructed by some surface (in which case the patch is in shadow), or it is marginal to some object. In the last case, the shadow pyray splits into four sub-pyrays, and the process continues with the sub-pyrays. As in the case of a regular pyray, the decision to split or not to split the marginal sub-pyrays is based on the same criterion as before. Subdivision can continue down any predetermined level (such as MAX or another user-supplied value).

The intensity of the light from the source is taken as the maximal intensity multiplied by the fraction of the areas of the shadow sub-pyrays that reach the patch. This shadow calculation is accurate to the user-prescribed ε. Strictly speaking, it should be noted that when the surface is curved, the shadow calculation described above cannot be completely accurate, because the shadow pyray may not intersect the surface at exactly the same patch.

A special case occurs when the original pyray splits into sub-pyrays due to marginality. Consider only those sub-pyrays that do not split any further (either because they are entirely in, entirely out, or have stopped splitting due to the stopping criterion or the level MAX). Those sub-pyrays that are entirely in the surface are treated as explained above, and those that are entirely outside are ignored. Consider now a sub-pyray which is marginal. Recall that in this case, a sample point in the patch (the center or a point jittered from the center) is used to sample the surface: if the sample point is in the surface, the entire patch is considered to be in the surface. In this case, the shadow is determined simply by casting a shadow ray from the sample point towards the light source. Since the patch is small and the shadow value of the original pyray is determined by all its sub-pyrays, we get an antialiased shadow also at the boundaries of objects.

4.2. Distributed Light Sources

There are two separate issues here: one is the creation of penumbrae (partial or "soft" shadows) from distributed sources, and another is the problem of antialiasing. In most cases the partial shadow itself does a sufficiently good job of antialiasing the shadow, but there are cases when it does not. We first discuss the creation of penumbrae under the simplifying assumption that we are only concerned with the shadow intensity at the exact point where the pyray's axis hits a surface.

Assume first that the source is a rectangle. Then, from the surface point that needs to be lit, create a *shadow* pyray with bounding rays aimed at the four corners of the rectangle. This is illustrated in Figure 4. We need to find the fraction of the shadow pyray that reaches the light without being obstructed. Again, this is done as described previously for a regular pyray, with a shadow pyray splitting when it is marginal with respect to an object. The shadow sub-pyrays (and their areas) that reach the light source determine the fraction of light that illuminates the surface point. If the light source is not rectangular, we first surround it by a bounding rectangle, and proceed as above. Next, we consider only the shadow sub-pyrays that hit (or are marginal to) the bounding rectangle. Each of these is either completely inside the light source itself, completely out, or marginal to the light. The shadow sub-pyrays that are marginal to the light are split according to the same principles.

The intensity of the light that we assign to each shadow sub-pyray hitting the light source is taken as $IA\cos\theta$, where I is the intensity of the source per unit

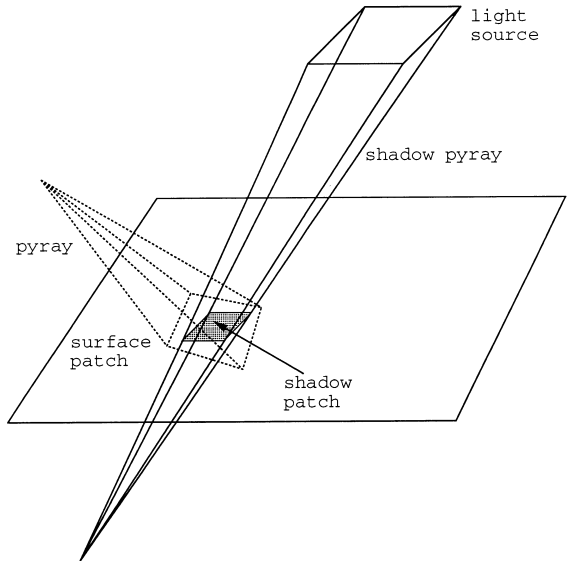

Figure 5: *Extending the shadow pyray for improved sampling.*

area (assumed constant for the source), A is the area of the source subtended by the shadow sub-pyray, and θ is the angle between the normal to the source and the axis of the shadow sub-pyray. This is the effective illumination for that particular shadow sub-pyray, since $A\cos\theta$ is the approximate area of the projection of the subtended area on a plane perpendicular to the shadow sub-pyray. In radiosity techniques, this is one way of approximating the form factors[20]. The intensity is also attenuated by the distance in the usual way[20].

Spherical light sources may also be simulated by simply omitting the $\cos\theta$ factor, which gives a disk perpendicular to the line of sight. From the point to be lit, a shadow pyray towards the center of the sphere is created with bounding rays defined by the radius of the sphere. The process would then proceed as above to find the percentage of light that makes it to the point.

What we have described above is correct only for a single point on the surface. We can use the single point as a sample for the shadow effecting the entire pixel, but there are cases where it could lead to aliasing errors. Figure 14 demonstrates this problem on the gazebo in the extreme right corner where the pyray axis makes a very small angle with the surface. The centers of adjacent pyrays are far apart on the surface, and the intersections of their respective shadow pyrays with other objects may be very different, resulting in sharp changes in shadow intensities. The inset in the figure is a 4×4 blow-up of the problem. Five solutions to this problem are outlined below.

4.3. Forced Subdivision

This method is the one we use with texture-mapped surfaces—see Subsection 3.2. Each pyray is forced to subdivide up to the user-supplied level TR (texture resolution). The effects of different values of TR can be seen in the insets of Figures 14 and 15.

4.3.1. Supersampling

Instead of creating just one shadow pyray from the center of the patch, we can choose more sample points within the patch, and take the shadow as the average of the results. We can also jitter the sample points. The user can vary the number of sample points and there is an obvious trade-off between accuracy and running time.

4.3.2. Extending the Shadow Pyray

The shadow pyray described above emanates from a surface point and its axis is a line joining the surface point and the center of the light source (the intersection of its diagonals). Now instead of taking this as the shadow pyray, we move the source of the pyray *behind* the surface. Now the shadow pyray intersects the surface in a patch, which we call the *shadow patch*. This idea is illustrated in Figure 5, and it is similar to the idea of defocusing (see next section). The original patch and the shadow patch obviously overlap, but they are usually not identical.

One problem that remains to be resolved with this approach is how large should we make the shadow

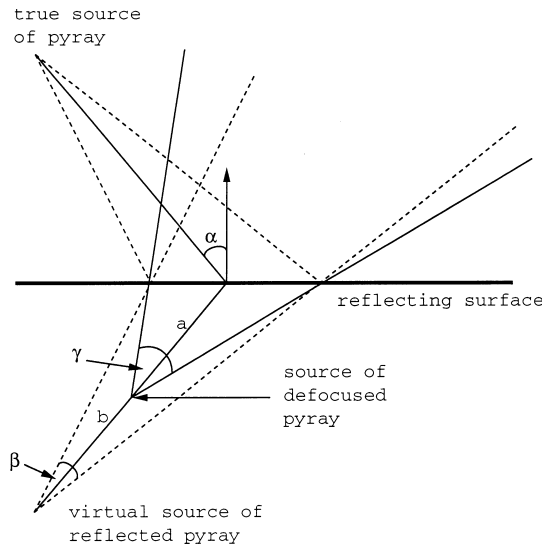

Figure 6: *Defocusing a reflected pyray to produce blurred reflections.*

patch? We want to make the shadow patch as large as possible so that it will sample the original patch as best as possible, but the shadow patch should not extend beyond the original patch, or we might get false shadows. Geometrically, this problem is identical to the following: consider the patch as a screen and the pyray's origin as the viewpoint. Our problem now is to move the viewpoint until the projection of the light source (towards the viewpoint) is maximal and still contained in the screen. Note that if the projection of the light source on the patch is small, we may have to move the source of the shadow pyray *behind* the light.

Our current implementation uses this method (except for textured surfaces, where we use forced subdivision).

4.3.3. Extension and Subdivision

This is a combination of two previous methods: we subdivide the original patch into sub-patches, and for every sub-patch we create an extended shadow pyray as described above. Clearly, this method requires less subdivisions than the simple subdivision approach, and the results are more accurate. The subdivisions can be done to any user-prescribed level.

4.3.4. Extension and Adaptive Subdivision

This method is the most consistent with our adaptive supersampling approach, but it involves some initial extra steps which may be time-consuming. We assume that the light is a rectangle—otherwise we surround it by a rectangle and handle the shadow (sub-)pyrays as described above. The first step is to project the light rectangle onto the same surface as the patch. This projection is done parallel to the line from the patch's center to the light's center. We then check to ensure that the entire patch lies inside this projection (it is sufficient to check that the patch's corners are inside). If it is not completely inside, we subdivide the patch into four and proceed with every sub-patch. In most cases, the patch will be inside the light's projection.

Assume now that we have a surface patch (or sub-patch) that is entirely inside the light's projection. We create a shadow pyray whose axis is the line joining the centers of the patch and the light, and whose source is so far behind the patch that the entire patch is *inside* the shadow ray (the corners of the shadow pyrays are aimed at the light's corners). We now trace the shadow pyray, with the patch as the first polygon, but we only trace the part of the shadow pyray that is *inside* the patch. Clearly, the shadow pyray will subdivide along the boundary of the patch. Another way of looking at it is as if the shadow pyray was a regular pyray and the patch was a hole in the surface. The shadow sub-pyrays that are inside the patch are traced towards the light, and the marginal ones are subdivided up to the ε accuracy or up to the MAX level.

To increase the efficiency of the above method, the actual order of tracing the shadow pyray is different. The shadow pyray at first ignores the patch in order to create the list of objects that it hits. This list is passed on to its shadow sub-pyrays and eliminates many objects from consideration while tracing the shadow sub-pyrays (see Section 6).

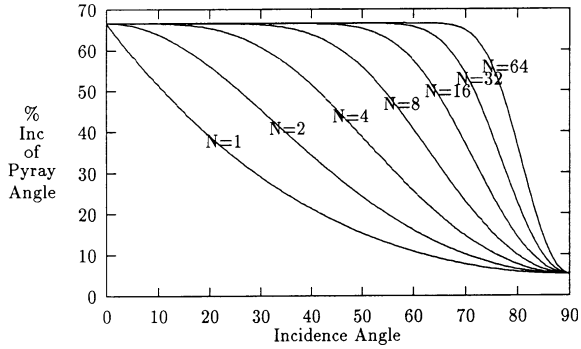

Figure 7: *Percentage increase of angle of defocused pyray over original angle of pyray (taken as 2°), plotted as a function of the incidence angle, for various values of N, with DFRMIN=0.6 and DFRMAX=0.95.*

5. Reflections

Sharp reflections of a pyray off a polygonal surface are straightfoward. In the next two subsections we deal with fuzzy or blurred reflections and with the problem of curved surfaces.

5.1. Blurred Reflections

Regular ray tracing handles the problem of fuzzy (or specular) reflection of a point light source very well. However, fuzzy reflections of other objects and distributed light sources require the more sophisticated methods outlined in Section 2. This anomaly is clearly seen in the early ray traced images: reflections of point light sources are fuzzy, whereas reflections of other objects are sharp. Both Phong's model and the Torrance-Sparrow model[20] assume that light sources are *points*, and as such, it is difficult to use them for distributed light sources. In our approach, all reflections (of lights and other objects) are treated in a similar manner. Stochastic sampling[10, 23] solves the same problem by distributing the reflected rays, but this requires a high degree of supersampling.

Another difficulty is the well-known phenomenon that most surfaces reflect in a manner that is dependent on the angle of incidence. Figure 19 shows this: a house is seen reflected from a surface, and the viewpoint is assumed to be close to the surface. The bottom part of the house is almost perfectly reflected, while the top part is very fuzzy. As explained in[27], the difference in fuzziness is due mainly to the difference in the viewing angle. Another contributing factor is the dependence of the fuzziness on the wavelength.

Our model of a solid reflected pyray allows a very simple solution to all of the above problems. Reflections of all types, and not only light sources, can be made fuzzy. Furthermore, the *degree of fuzziness* can depend on the angle of incidence and the wavelength, and the user can specify this dependency. The drawback of our simple method is that it is not based on a physical model, and hence requires experimentation and tuning to give accurate results.

Our solution is best explained by examining the geometry of a reflected pyray, as in Figure 6. The pyray, if reflected from a perfect mirror, behaves geometrically as if it emanated from a point which is a reflection of the pyray's source. To introduce fuzziness into this scheme, we *defocus* the reflected pyray by shifting the reflected source forward along the axis of the pyray. The effect is that the reflected pyray subtends a wider angle, and thus adjacent pyrays overlap after the reflection. This overlap of adjacent pyrays causes points to be reflected in more than one pyray, and this produces an overall fuzzy appearance.

In Figure 6, we denote the angle of incidence by α, the angle of the pyray by β, and the angle of the foreshortened pyray by γ. We also denote the ratio of the distances between the two sources of the pyrays and the surface by DFR (the defocusing ratio); in Figure 6, DFR=a/b. Note that this ratio is always between 0 and 1. In order to model the dependence of the *fuzziness* on α, our general model calls for the DFR to be some function of α, depending on the surface. One simple function that suggests itself is to select a minimum and maximum value for the DFR—call them DFRMIN and DFRMAX—where the minimum is for $\alpha = 0°$, and the maximum is for $\alpha = 90°$. For other values of α, DFR=DFRMIN+(DFRMAX-DFRMIN)$\sin(\alpha)^N$, where N is a parameter controlling the rate at which the DFR varies.

The DFR is very easy to use in modeling the defocusing idea, but its value is not a very good indication of the degree of fuzziness of the reflection. A more natural measure for this fuzziness is simply the percentage in-

DFRMIN	0.1	0.2	0.3	0.4	0.5	0.6	0.7	0.8	0.9
$100(\gamma-\beta)/\beta$	890%	399%	233%	150%	100%	67%	43%	25%	11%

Table 1: *Percentage Increase of Pyray Angle for Different Values of DFRMIN ($\alpha = 0°$)*

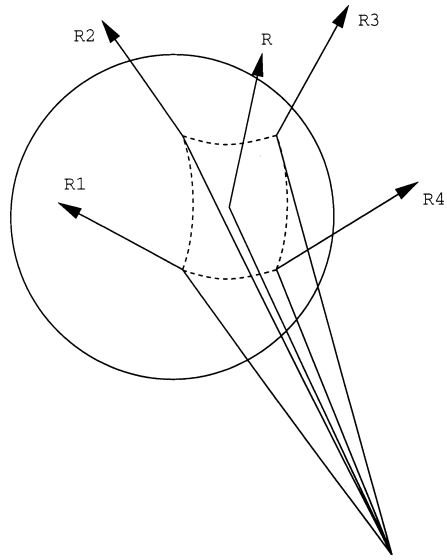

Figure 8: *A pyray reflected from a curved surface.*

crease of the wider pyray angle over the original pyray angle, i.e., $100(\gamma-\beta)/\beta$. Figure 7 shows plots of this percentage increase as a function of the incidence angle α, for DFRMIN=0.6, DFRMAX=0.95, $\beta = 2°$, and several values of N. Other values of the parameters produce essentially similar graphs. Of course, a DFR close to 1.0 produces sharp reflections (small percentage increase of γ over β).

Clearly, a lot of field work is called for to determine which values of the parameters DFRMIN, DFRMAX and N best model the different types of surfaces that occur in everyday environments. Table 1 is given as an aid in choosing DFRMIN; it shows the percentage increase of the pyray angle for different values of DFRMIN, for $\alpha = 0°$.

Another issue is that the fuzziness also depends on the wavelength[27]. This can be easily incorporated into our model by selecting three different DFR's for red, green and blue. Although it might appear that such a solution should take three times as long to implement, that is not the case. By first doing the widest pyray, its list of marginal objects (see next section) can be passed on to the pyrays of the other two wavelengths, resulting in very considerable time savings.

Most surfaces exhibit fuzziness that is not uniform (even for a constant angle of incidence), due to the uneveness of the surface. This uneveness can also be modeled by our defocusing method by first computing a DFR according to the above model, and then perturbing this value according to some distribution function. Similar effects were studied in[17, 23], but we have not implemented them in our present work.

5.2. Reflections Off Curved Surfaces

Our approach to antialiasing of curved surfaces is basically similar to that of polygons: when a pyray is marginal to a curved surface, it splits into sub-pyrays, and the process continues until either the stopping criterion is satisfied, or the level MAX is reached. The values of sub-pyrays that are still marginal (but do not split further) are determined by a single sample point. In the following discussion, "pyray" refers to an original pyray or a sub-pyray that is not marginal and needs to be reflected from a curved surface.

Reflections of a pyray off a flat surface are simple, because the reflection of a pyray is, geometrically, also a pyray. The problem is that of reflections off a curved surface, such as a sphere. Firstly, the four reflected cor-

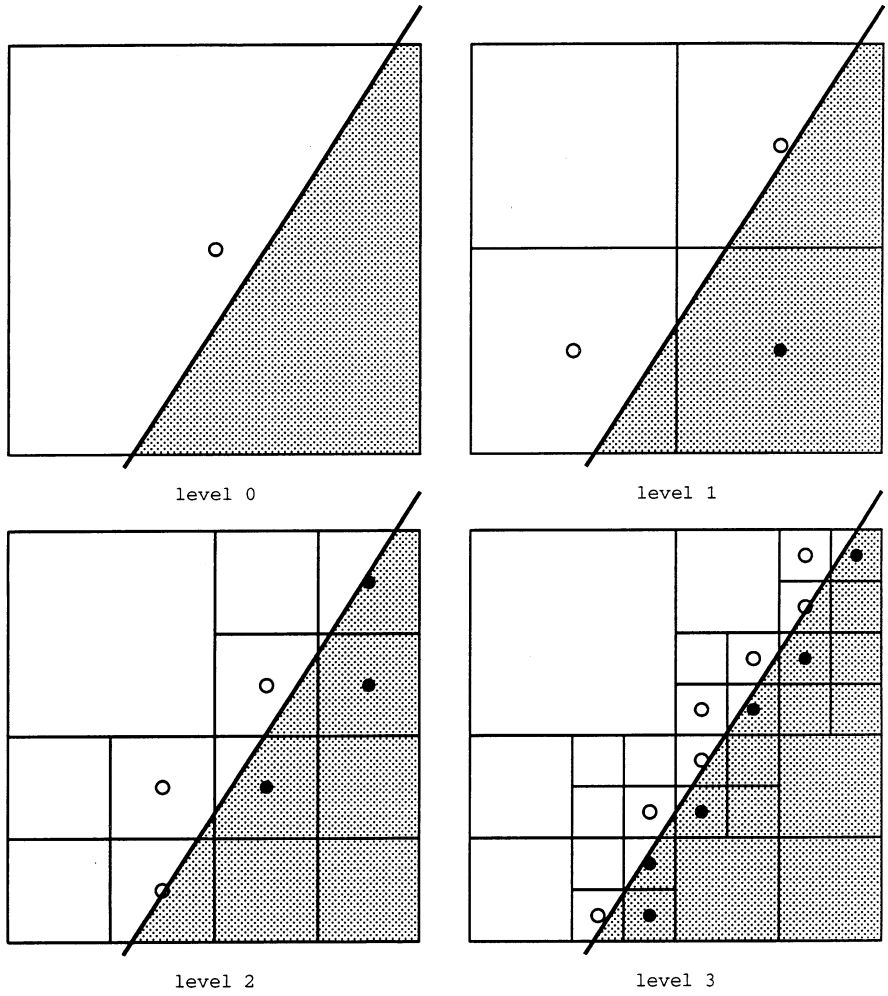

Figure 9: *Intersection of object and pyray with one marginal edge, showing adaptive subdivision at levels 0 to 3.*

ners of the pyrays no longer meet at a single point. Secondly, the reflection of the side of the pyray is no longer planar but curved. And lastly, the reflection of the pyray may now subtend such a wide angle that it is no longer manageable. We propose four different solutions to these problems, each having its own advantages and disadvantages.

5.2.1. Approximating the Reflected Pyray

In this approach, we approximate the reflected pyray provided its angle is not too wide. Figure 8 illustrates this method. When a ray is reflected off a curved surface, we consider the four rays, R1, R2, R3, R4, which are the reflections of the bounding lines of the original pyray. Each of these four rays is defined by a point on the surface and a direction vector. Since the reflection of the pyray is *not* a pyray, we construct a pyray to approximate the reflection. Before doing that, we check the maximal angle between opposite pairs of rays from R1–R4, and if it is wider than some user-specified value, we subdivide the pyray. This subdivision can continue up to the level MAX. At the level of MAX, we just sample the sub-pyray by its axis (or by a jittered displacement of the axis). In the following, we assume that the pyray we are dealing with is already narrow enough not to be split.

For the approximation, we need to determine a source and an axis, and this is done as follows. The source of the approximating pyray is taken as the point in space such that the sum of the squares of its distances to R1–R4 is minimal. The axis of the approximating pyray is now taken as originating from this source and going through the point at which the axis of the original pyray hit the surface. This ray is called R in Figure 8. The four corners

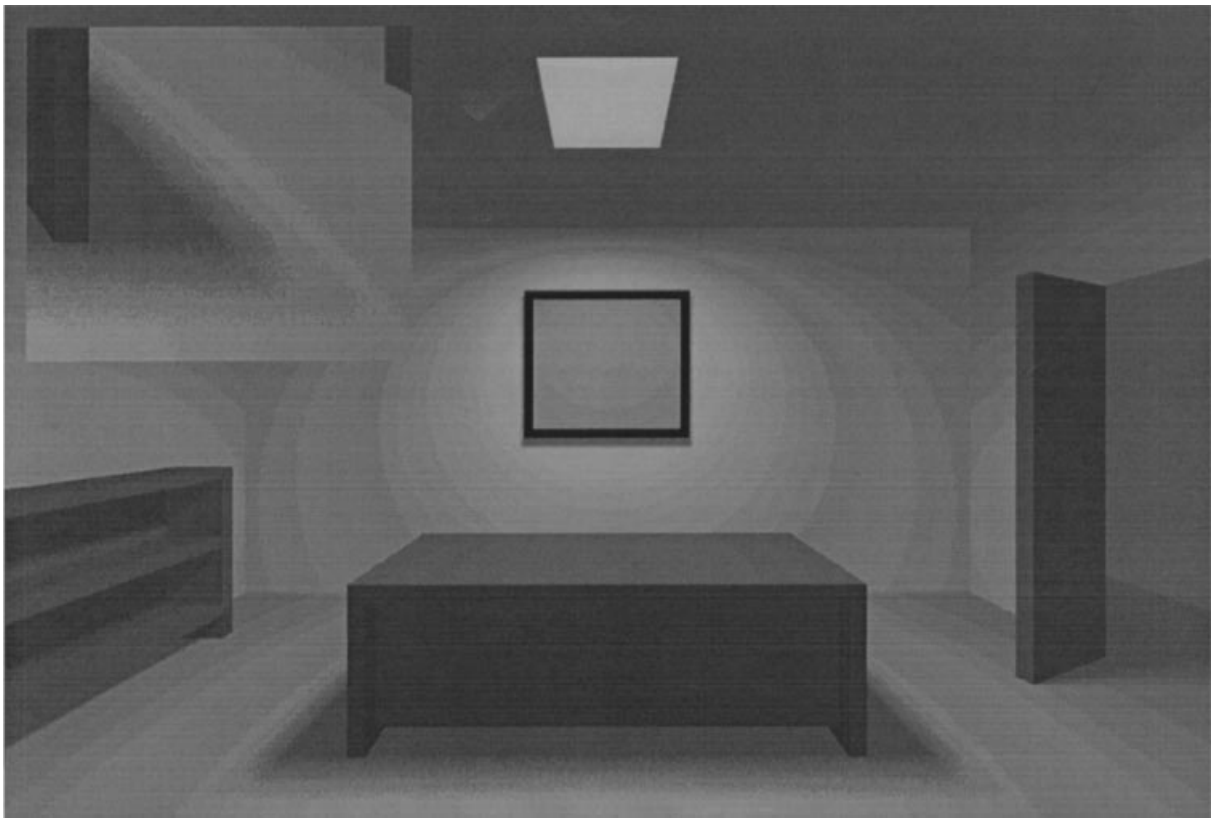

Figure 10: *Stochastic sampling, 16 rays per pixel; quality: poor; time: 73.70 min.; time for similar image using ASOS: 23.65 min.*

of the approximating pyray are taken as emanating from the source and passing through the four points at which the corners of the original pyray hit the surface. We now continue to trace with the approximating pyray, which can also be defocused like a regular reflected pyray.

This technique is quite straightforward, but the required calculations can be time-consuming to such an extent that another approach might be better. Another problem is that the approximating pyray is still just an approximation, and it may result in certain anomalies. For example, in some cases, the approximations of adjacent reflections may overlap, and in other cases, such approximations may miss certain volumes in space. Another problem is the determination of the threshold angle: if it is too large, the anomalies might show up as artifacts, and if it is too small, then we could be wasting time on calculations which just end up with a decision to split the original pyray.

5.2.2. The Tangent-plane Method

This is the simplest solution. At the point where a pyray's axis hits the surface, we reflect the pyray about the plane tangent to the surface at that point. This plane is easily derived from the point of contact and the normal at that point.

The obvious problem with this approach is that adjacent pyrays will be reflected in such a way that certain volumes between pyrays will be missed. However, this problem can be remedied to some extent by defocusing the pyrays as explained in the previous subsection.

It should also be noted that the images obtained by this approach cannot be worse than those obtained when all curved surfaces are approximated by polygonal meshes (a very common approach to rendering curved surfaces). What we are doing here is, in effect, a local replacement of the curved surface by a very small polygon, namely, the pyray's intersection with the tangent plane. The advantage of this approach over an ordinary polygonal approximation is that it is always done at image resolution, so rendering a close-up view of a curved surface will never reveal any polygonal structure.

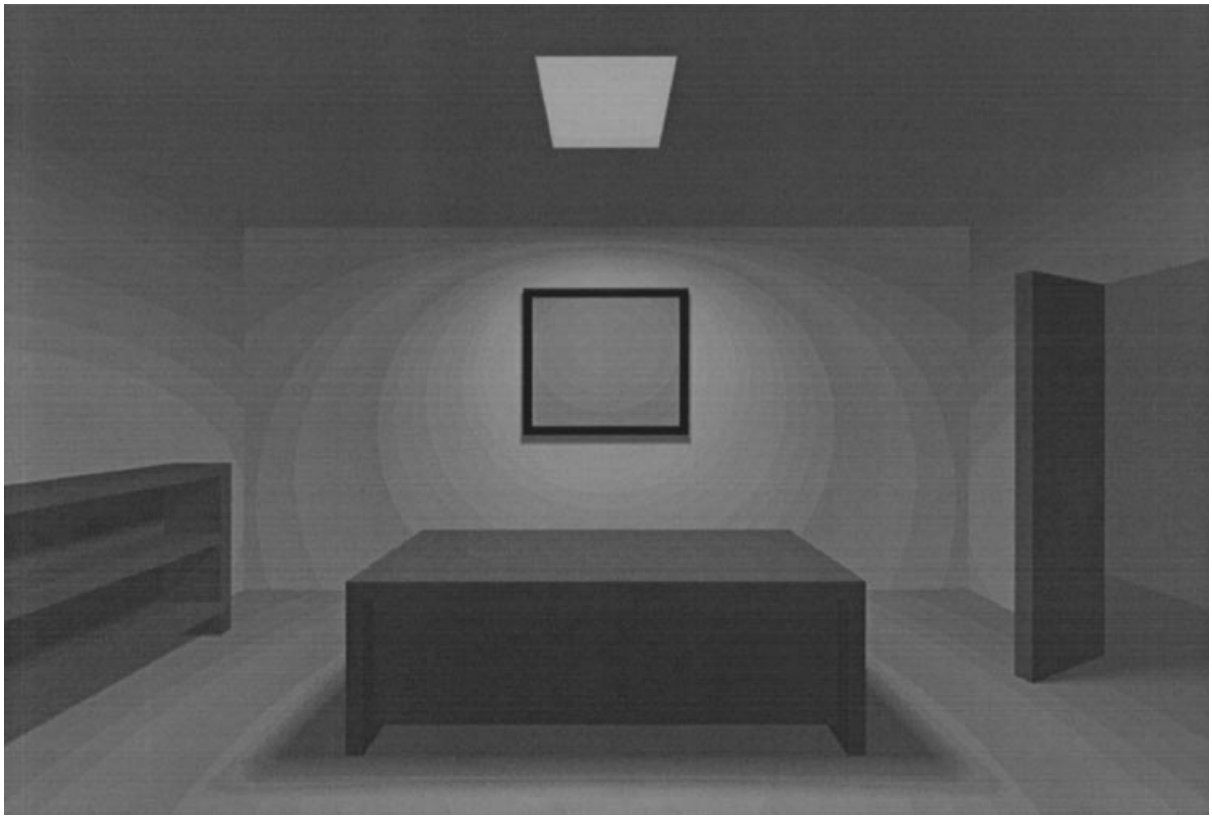

Figure 11: *ASOS (MAX=3, ε=1/8); quality: good; time: 27.71 min.; time for similar image with stochastic sampling: 383.10 min.*

5.2.3. Curved Reflections by Supersampling

This solution takes more time than the previous one but is more accurate. Whenever a pyray hits a curved surface, it splits up to some predetermined maximal level, and we simply continue to trace each of the sub-pyrays separately. For the sub-pyrays, their reflections off the curved surface are done by the tangent-plane method outlined above. This approach ensures that the scene will be sampled much more uniformly and with much smaller gaps than with the tangent-plane approach. Furthermore, if we want to do texture mapping on the curved surface, we have to adopt this solution since we have no other way of antialiasing the texture map.

5.2.4. Curved Reflections by Adaptive Supersampling

This is a refinement of the previous method, and it is keeping with our principle of adaptive supersampling. When a pyray is reflected off a curved surface, we test the widest angle that is formed between R1–R4 (see Figure 8). If that angle is greater than some user supplied threshold, we subdivide the pyray into four sub-pyrays, and repeat the procedure with every sub-pyray. If the angle is less than the threshold, the (sub-) pyray is reflected by the tangent-plane method, and it can also be defocused in the regular way. The subdivision can continue up to some user-specified maximal level.

6. Efficiency Considerations

In this section, we discuss several matters relating to efficiency.

6.1. Hit Lists

When a 0-ray is intersected with the scene, a list containing all of the objects it hit or was marginal to is returned. Since a sub-pyray can only be marginal to an object if its parent was marginal, the sub-pyray only has be intersected with the hit list of its parent instead of the entire scene. This method considerably speeds up the process, even when we subdivide *all* pyrays.

When a pyray is marginal to a polygon, it may be marginal to more than one edge. Clearly, none of its sub-pyrays can be marginal to any other edges, so in

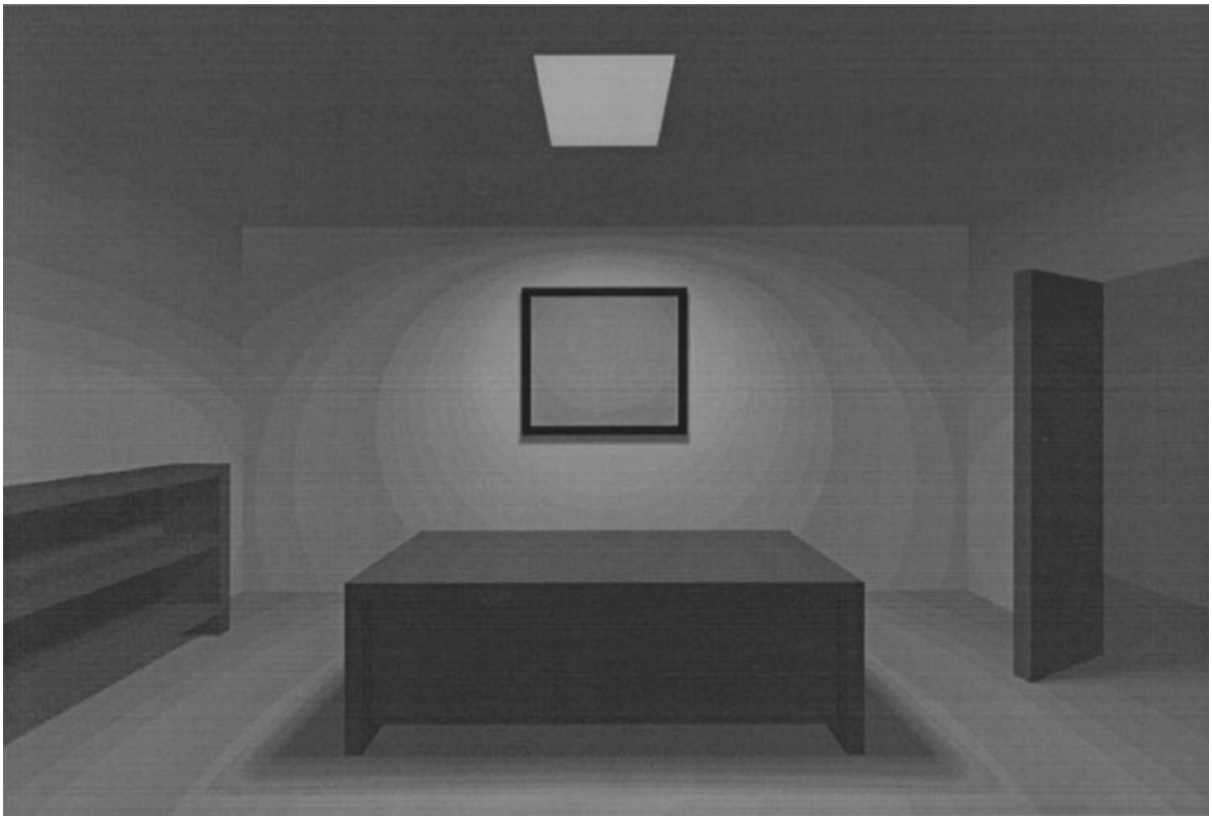

Figure 12: *ASOS (MAX=4, ε=1/8); quality: very good; time: 35.98 min.*

order to minimize computation time, the information about the marginal edges can be passed from a pyray to its sub-pyrays. We can maintain a list of all the edges of the polygon which are close to the pyray. When the sub-pyrays are considered, we need only compare them with the edges on this list (and not all edges of the polygon). Note, however, that the order in which a pyray intersects some marginal surfaces is not necessarily identical with the ordering for its sub-pyrays.

6.2. Proximity to One Edge

When a ray is in proximity to just one edge, we can improve our stopping criterion by observing that for each marginal K-ray, at most half of it can switch from *in* to *out* (or from *out* to *in*). The reason is that if the center of a K-ray is *in*, then at most 2 of its (K+1)-subrays can be *out*. Therefore, in the decision criterion, L can be replaced by L/2, giving us the modified criterion of:

If $L \leq 2^{2K+1}\varepsilon$ then stop subdividing (the marginal rays).

This would, on the average, require many fewer subdivisions than the previous criterion, because in a polygonal object, almost all marginal rays would be in proximity to just one edge.

Figure 9 shows a ray in proximity to just one edge. We use $\varepsilon=1/16$ as before. So now we must compare L with $2^{2K+1-4} = 2^{2K-3}$.

K=1 M=3, IN=1, OUT=2 so L=2. $2^{2K-3} = 1/2 < L$ so we subdivide the marginal 1-rays.
K=2 M=6, IN=3, OUT=3, so L=3. $2^{2K-3} = 2 < L$ so we subdivide the marginal 2-rays.
K=3 M=13, IN=6, OUT=7, so L=7. $2^{2K-3} = 8 > L$ so we stop at this stage.

In the case of a single edge, we can easily compute an upper bound on the depth of subdivision K required for a given ε. Note that no matter how the edge intersects the original 0-ray, the maximum value for L is just 2^K (the original square can be seen as a 2^Kx2^K array of K-rays). So in order for the modified criterion to hold, it is sufficient to have $2^K \leq 2^{2K+1}\varepsilon$, i.e., $K \geq log_2(1/\varepsilon)-1$. For example, if $\varepsilon=1/16$, we will always stop with K=3 (or less, depending on L).

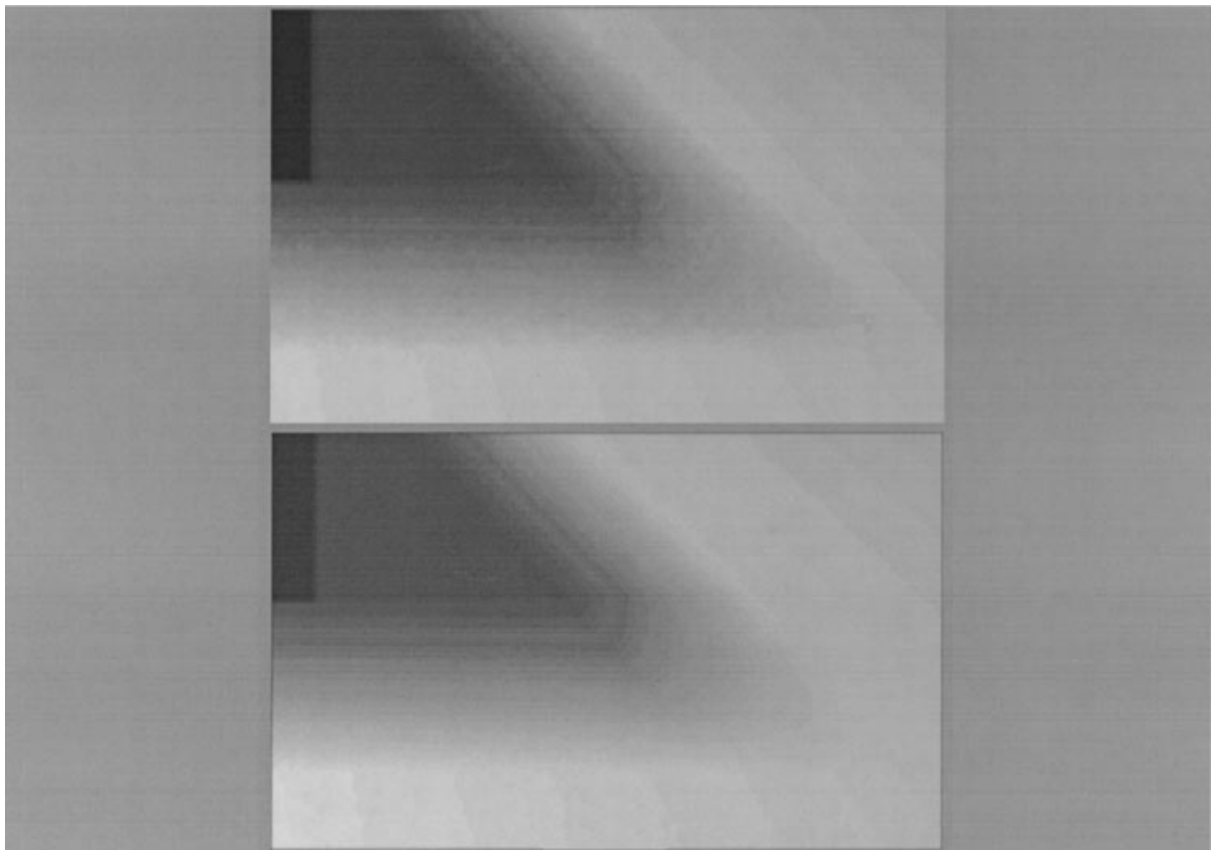

Figure 13: 4×4 *blowup of previous images, showing difference in penumbrae.*

6.3. Using Hierarchical Data Structures

The use of hierarchical data structures to speed up ray-object intersection is widely prevalent. Many schemes have been proposed, and at their basis lies the fact that the intersection of a ray and a bounding volume is easy to compute. A natural question that arises is how can these schemes be extended to pyrays.

Pyrays can use such data structures very easily. Our technique for splitting pyrays adapts ideally as follows. Consider a pyray (or a sub-pyray) and a bounding volume: it either misses the bounding volume completely, or the entire pyray is within the bounding volume, or the pyray is marginal to the bounding volume.

Clearly, the first two cases can be handled in a straightforward manner. In the third case, the pyray splits in the usual manner, and we consider each sub-pyray separately. Splitting can continue recursively until we either reach MAX (maximal level of splitting), or our stopping criterion is satisfied. At the lowest level, the pyray is sampled by a single ray in the usual manner.

We have not implemented the interaction of pyrays and hierarchical bounding volumes, but the implementation is the same as the regular interaction of a pyray and a box or parallelpiped or sphere.

6.4. Other Speed-up Methods

The entire sampling process may be sped up by initially sampling pixels in clusters, such as 2×2, 3×3, or 4×4. If such a "fat" pyray is marginal, we just split it up, and pass the hit list to its sub-pyrays. Note that if the cluster size is not a power of 2 then splitting has to be done differently. If the fat pyray is not marginal, we can use this value for each of its interior pixels, achieving a big saving in processing time. The bigger the cluster, the higher the potential savings, but the likelihood of image banding is higher. This idea is simply a way of using a lower resolution base.

Another efficiency consideration concerns shadow pyrays: when the light source is a simple rectangle and the shadow pyray is in proximity to only one edge or only one sphere (or some other simple prim-

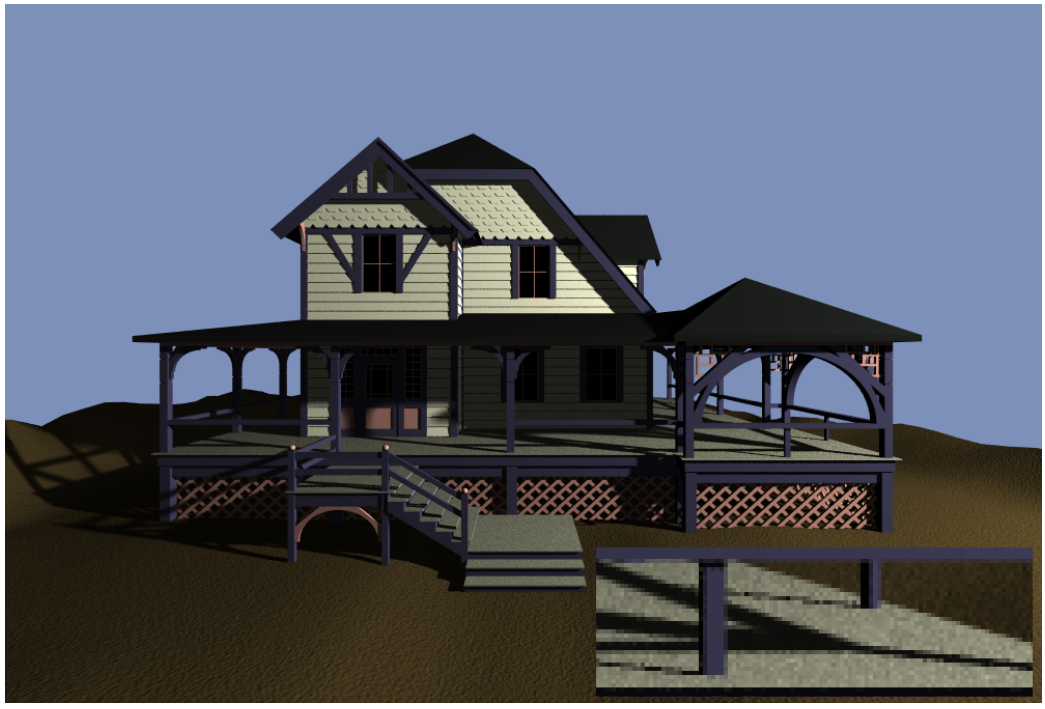

Figure 14: *House with texture mapping rendered with ASOS (MAX=2, ε=0) and texture sampled 4 times per pixel; quality: good; time: 158.01 min. Some shadow aliasing (enlarged) is noticeable.*

itive), we can avoid the subdivision process and calculate the fraction of the pyray that remains unobscured. This is similar to the approach of cone tracing. However, in other cases, the subdivision is necessary for calculating a good approximation to the correct shadow.

7. Results and Discussion

Our technique (ASOS) was implemented on a Silicon Graphics Onyx with a 150 MHz R4400 processor and all images were rendered at a resolution of 1000×675. We have implemented our scheme on polygonal objects, spheres, cylinders, and cones. The exact treatment of the pyray-object intersections is detailed in[15, 16]. For other curved surfaces, one would have to provide routines for detecting the proximity of a pyray to the boundary, intersection detection of a ray, and calculation of the normal at any point on the surface.

As for light sources, we have implemented point light sources, linear lights, spherical lights, and distributed lights from rectangles and arbitrary polygons. For shadows, we have done penumbrae, and have also implemented antialiasing of point and distributed sources. The antialiasing of distributed sources was done by the extended shadow pyray method (moving the source of the shadow polygon back so that the shadow pyray intersects the patch defined on the surface by the original pyray).

We have also implemented sharp and fuzzy reflections, including dependence of the fuzziness on the viewing angle. All reflections from curved surfaces (sharp and blurred) were implemented using the simple tangent-plane method, which proved sufficient for our images.

We have chosen to compare ASOS against stochastic sampling because the images are comparable in quality. We have not used the adaptive techniques mentioned in Subsection 2.5, since the adaptiveness is image-driven, with the same inherent problems as adaptive ray tracing (see Subsection 2.3).

7.1. Simple Images

Figure 10 was rendered with stochastic sampling, with 16 rays per pixel. The image took 73.70 minutes to render, and as can be seen, the penumbra from the desk is quite splotchy. A comparable image with ASOS (MAX=2, $\varepsilon=1/8$) took only 23.65 minutes.

Figure 11 was rendered with ASOS (MAX=3, $\varepsilon=1/8$) (i.e. subdividing up to a maximum of 64). This image is

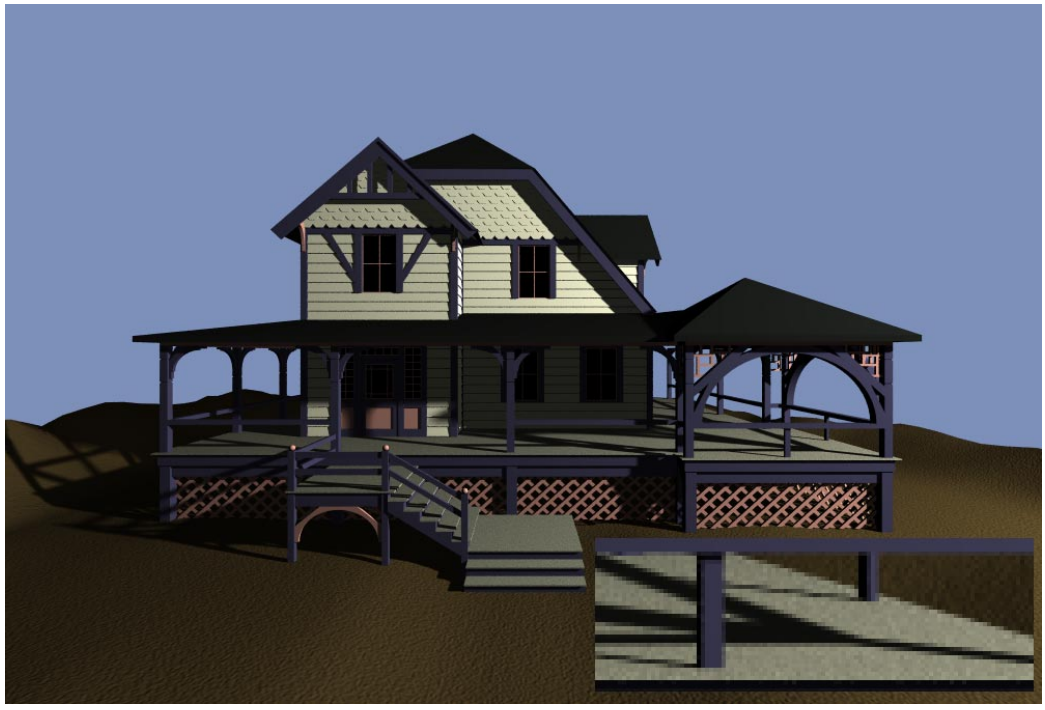

Figure 15: *Same as last, but texture sampled 16 times per pixel. Quality: very good; time: 353.55 min. Time for similar image with stochastic sampling: 539.42 min. Shadow aliasing is improved.*

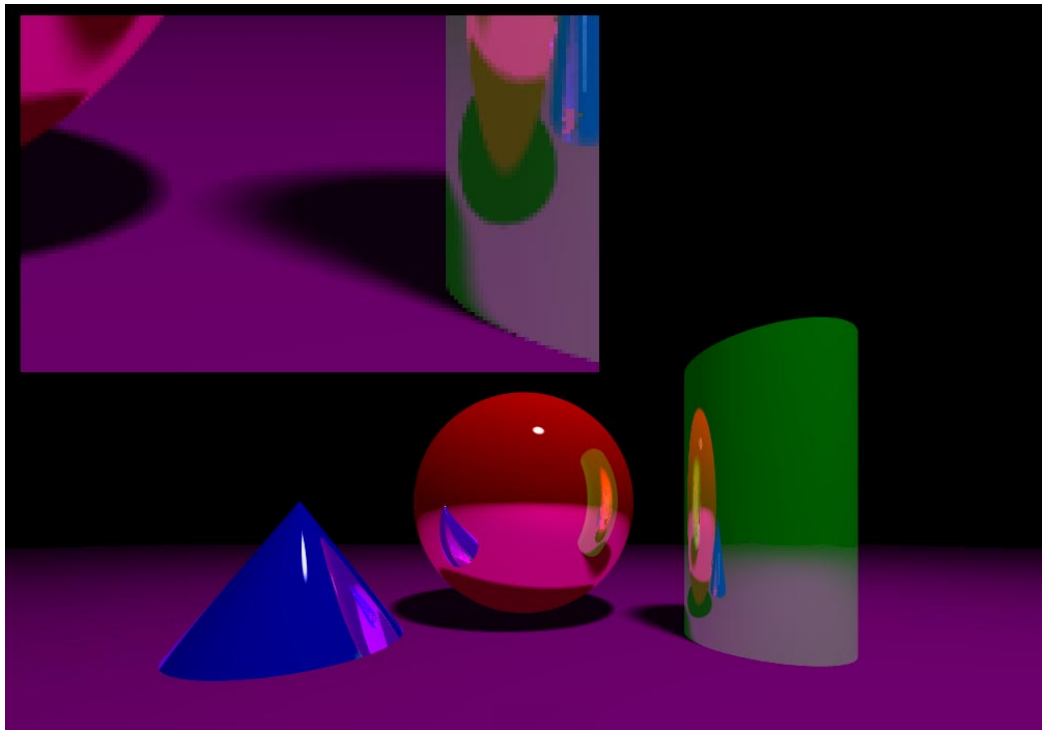

Figure 21: *Blurred reflections from curved objects.*

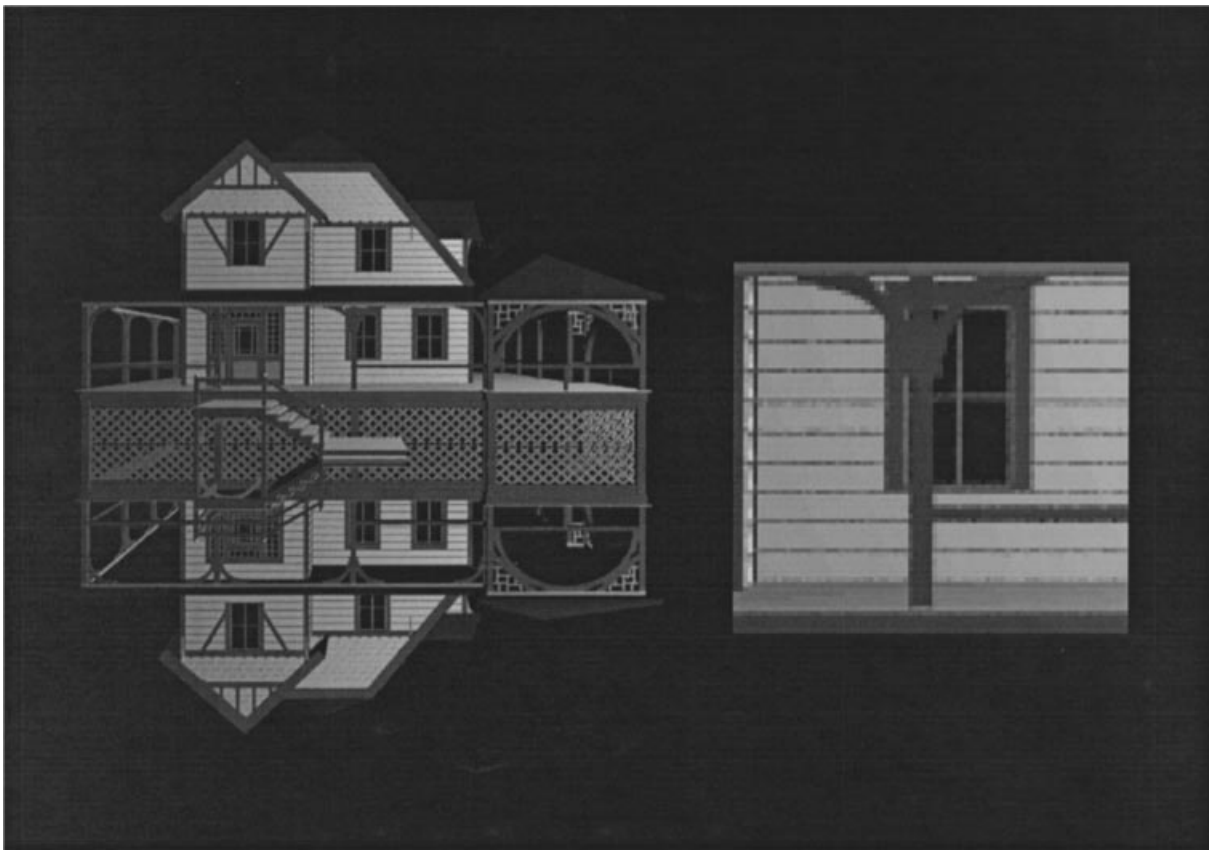

Figure 16: *House on reflecting plane rendered with ASOS (MAX=2, ε=1/8); quality: good; time: 49.19 min. Time for similar image using stochastic sampling: 308.26 min.*

obviously a big improvement over the previous one, and the time was only slightly more than ASOS required for the previous image: 27.71 minutes. A comparable image with stochastic sampling casting 64 rays per pixel and took 383.10 minutes.

At this point it is necessary to explain why such a big improvement required so little extra time. The reason is due to our technique of passing the polygon hit list from a (sub-)pyray to its sub-pyrays. Most of the time is spent on determining the hit list for the initial pyray, so splitting to a deeper level is relatively cheap.

Finally, Figure 12 was rendered with ASOS (MAX=4, ε=1/8). The penumbra from the desk looks perfect, and the time to render the image was 35.98 minutes. No attempt was made to render a comparable image with stochastic sampling. Figure 13 is a 4×4 blowup of a section of Figures 11 and 12 showing the improved penumbra.

7.2. House with Texture Maps

The images here consist of a house made up of 2,770 polygons. A spherical light source provides the light and bounding boxes were used around most of the objects to speed up the intersection calculations. The porch is rendered with a procedural texture map, and the ground consists of a triangular mesh made up of 1,139 triangles with a procedural sand bump map.

Antialiasing was achieved as described in Subsection 3.2. Both images were rendered with MAX=2 (i.e., the smallest sub-pyray was 1/16th of a pyray) and ε=0, forcing all marginal sub-pyrays to subdivide to level 2.

Figure 14 shows the image rendered with TR=2, i.e., non-marginal pyrays subdivided into 2×2, so the texture map was sampled 4 times by each pixel. The time for this image was 158.01 minutes, and the image quality is reasonably good for its size and resolution.

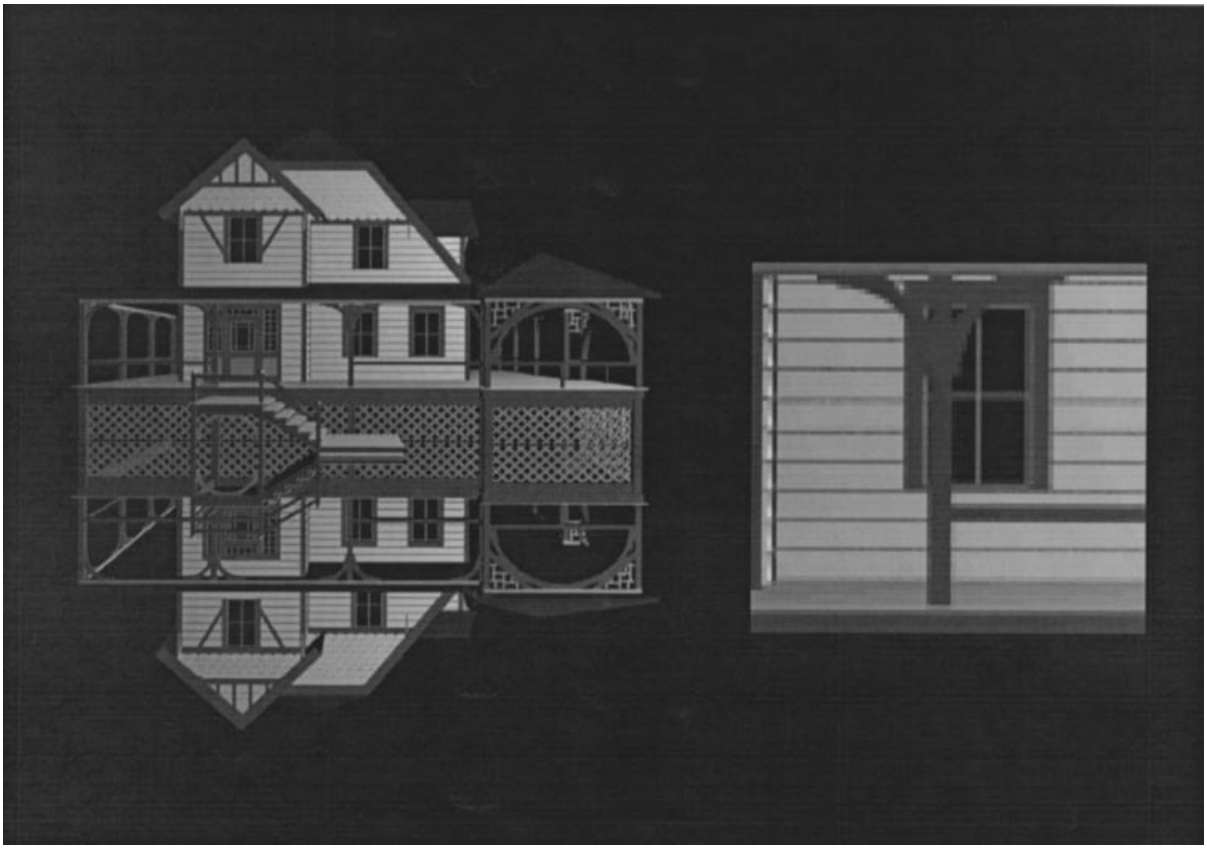

Figure 17: *Same as last, but MAX=3. Quality: very good; time: 92.25.*

Figure 15 shows the same image rendered with TR=4, meaning that the texture map was sampled 16 times per pixel. This image took 353.55 minutes, and the image quality is very high. A comparable image by stochastic sampling was obtained by sampling each pixel 16 times, requiring 539.42 min., or approximately 50% more time. The main reason that the time savings here are not as dramatic is that when a non-marginal ray hits a textured surface, it not only samples the texture 16 times but also sends 16 shadow rays to the light source.

The insets of the figures are a 4×4 blow-up of the extreme right corner of the gazebo. They show in detail that a higher TR improves the antialiasing of both the texture map and the shadows.

7.3. House with Reflections

The same house as above is shown here set on a reflecting plane without any texture maps or shadows. In the first two images the plane is a perfect reflector, and in the other images the plane creates blurred reflections with the fuzziness depending on the viewing angle.

Figure 16 shows the house rendered with ASOS (MAX=2, ε=1/8). The time for this image was 49.19 minutes, and the image quality is reasonably good. A comparable image with stochastic sampling, with 16 samples per pixel took 308.26 minutes. These timings indicate that even for images with many polygons, ASOS can achieve a dramatic time savings over stochastic sampling.

Figure 17 shows the same image rendered with ASOS (MAX=3, ε=1/8). The improvement in this image is noticeable on the screen, but it is slight. When portions of both images are blown up, there is quite a noticeable difference. The time for this image was 92.25 minutes, and a comparable image with stochastic sampling would have required 64 rays per pixel was not attempted.

Figures 18 and 19 show the effect of blurred reflections, with the amount of blur depending on the viewing angle. For both images, DFRMIN=0.05, DFRMAX=1.0, ε=1/8 and MAX=3. The parameter N was 32 and 64 respectively, showing the effect of N on the rate at which the blur changes with the viewing angle. As N increases, the range of viewing angles at which the

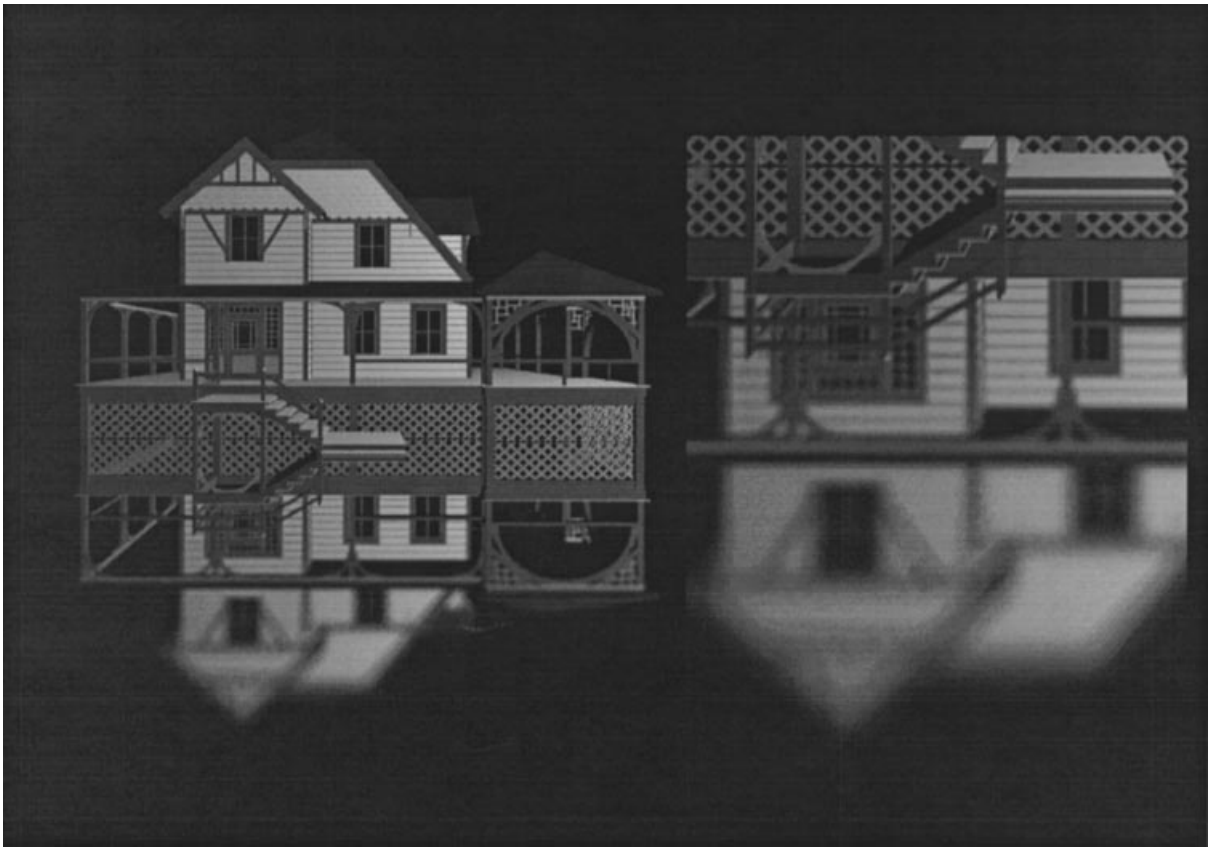

Figure 18: *Blurred reflections using ASOS (MAX=3, ε=1/8, DFRMIN=0.05, DFRMAX=1.0, N=32); time: 182.83 min.*

blur is noticeable also increases. Figure 18 took 182.83 minutes and Figure 19 took 225.90 minutes.

7.4. Images with Secondary Reflections

Figure 20 shows the office scene with the camera moved closer to the desk and the desk made metallic. This images was rendered with ASOS (MAX=3, ε=1/8) in 28.74 minutes and shows a blurred reflection of the whiteboard on the top of the desk. Also note reflection of the light off of the whiteboard as well. Figure 21 (see p. 47) shows a sphere, cylinder and cone sitting on a non-reflective plane. This image was rendered with ASOS (MAX=3, ε=1/8) in 2.48 minutes while allowing 6 reflective bounces.

7.5. Summary of Results

Table 2 summarizes our qualitative and quantitative results, using ASOS and stochastic sampling.

Qualitatively, one can summarize these results by saying that ASOS achieves a speedup by an order of magnitude over stochastic sampling when no texture mapping is involved. Even with texture maps, stochastic sampling can take some 50% more time to achieve comparable results.

8. Conclusions

We have introduced a new ray tracing technique for the problems of aliasing, handling distributed light sources, and generating fuzzy reflections. Both light sources and regular objects are blurred in the same uniform manner, producing either specular reflections of light sources, or fuzzy reflections of regular objects. We have also shown how to antialias shadows from distributed sources, which is a different problem than just creating soft shadows. Our method operates in object-space, and can be tuned to any desired accuracy. Note that our method of producing fuzzy reflections is not based on a physical model, and so it requires some tuning for different surfaces.

ASOS (adaptive supersampling in object space) can handle reflections from any curved surface, and we have

Figure 19: *Same as last, but with N=64, showing the effect of N on the blurred portions. Time: 225.90 min.*

implemented reflections—both sharp and fuzzy—from spheres, cylinders and cones. For other curved surfaces, the user would have to supply the routines for testing proximity, calculating intersection of a (line) ray and a surface, and deriving the normal to the surface at a given point.

The run times of our test images were mainly compared against those of stochastic ray tracing, since our method can be viewed as producing identical results to that method. (More efficient stochastic techniques are adaptive in image-space, and where not used in this research.) Test runs are extremely favorable to ASOS, and we can even produce better images in a shorter time. These time savings are mainly due to the fact that we supersample only at object boundaries, but even when we force ASOS to supersample large areas (as needed for antialiasing texture maps), we still get a big savings in time due to our method of passing the object list from a pyray to its sub-pyrays. Thus, ASOS can also be viewed as a useful acceleration technique.

Our method's ability to capture very small or thin objects makes it extremely useful for animation, because temporal aliasing can cause small objects to flash on and off. It is not enough just to detect such objects, it is also important to get a good approximation to their area, otherwise they may appear to pulsate with different intensities. The same can be said about small or thin shadows, and small gaps between objects. With ASOS, we can approximate such areas to any required precision.

The use of our technique does not preclude the application of other antialiasing methods. For example, stochastic sampling can be used for transparent objects. This combination of two techniques can be used to handle certain aliasing problems such as object intersections in CSG models. Another antialiasing method calls for sampling each pixel beyond the pixel area; this can be easily done by casting the original pyrays through a square larger than a pixel, though we have not studied this approach.

Although we do not solve the global illumination problem, several of the techniques that do so use ray

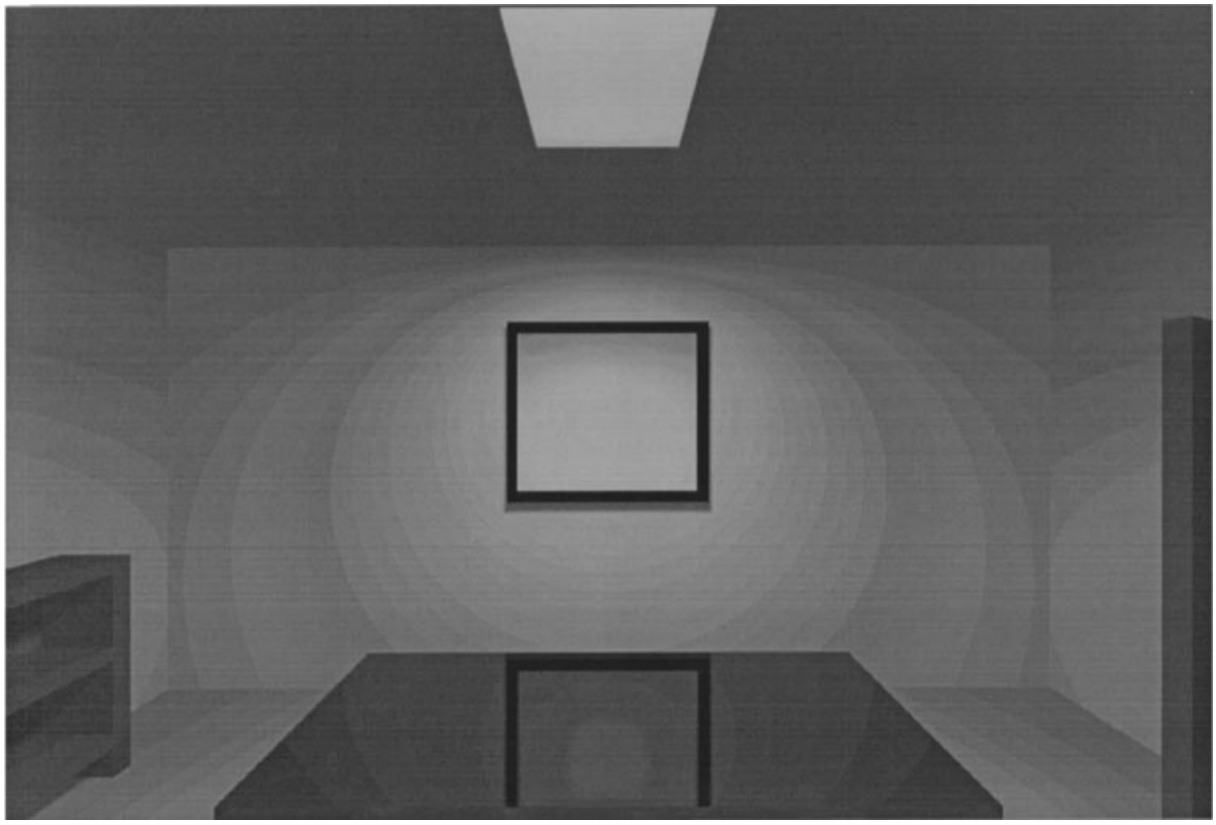

Figure 20: *Blurred reflections from one and two bounces.*

Figure	Image	Quality	ASOS Time	Stochastic Time
10	Office	Poor	23.65	73.70
11	Office	Good	27.71	383.10
12	Office	Very Good	35.98	n/a
14	House w/texture	Good	158.01	n/a
15	House w/texture	Very Good	353.55	539.42
16	Reflected House	Good	49.19	308.26
17	Reflected House	Very Good	92.25	n/a
18	Blurry (N=32)	Very Good	182.83	n/a
19	Blurry (N=64)	Very Good	225.90	n/a

Table 2: *Qualitative and Quantitative Results: ASOS and Stochastic Sampling*

tracing as an essential step. These methods could use ASOS to speed up and enhance the ray tracing part. ASOS can also be combined with regular stochastic sampling to handle the problem of refraction, for which at present we do not have a solution.

Future research in ASOS can be expected to deal with a variety of problems, some of which are outlined below:

- Refractions: The problem of transparent objects is a difficult one, particularly when distributed light sources are involved. The difficulty here is that we cannot aim a simple pyray towards the light source because of the refraction of light at the boundaries of the medium.
- Acceleration: The literature of ray tracing abounds with various acceleration techniques. Not all of them

are suitable for use with pyramidal rays, and studying the techniques that can be applied to ASOS should be an interesting research topic. Another topic that comes under acceleration is the handling of extremely complex scenes involving billions of polygons[12, 13].

- Rough environments: Many naturally occurring materials exhibit the property that light is blurred in a manner that depends not only on the viewing angle and wavelength, but also in a random manner. This effect can be modeled by two parameters. One is the surface normal, which can can be varied according to some distribution function, and another is the defocusing ratio, which can also be varied in a similar manner.
- Other blurring effects: It is quite easy to extend our defocusing method to handle other blurring effects. For example, depth-of-field effects can easily be modeled by simply defocusing the original pyray in a manner dependent on the depth of the object. Motion blur can also be done, but slightly differently: the pyray's source stays at the viewpoint, but now the *pixel* is distorted by elongating it in the direction of the object's motion; the amount of distortion should be a function of the depth of the object and its speed.

Acknowledgements

Portions of this research were carried out while the first two authors were at Texas A&M University. The authors wish to thank Susan Van Baerle and Sean Graves for several suggestions. Thanks are also due to the anonymous referees whose comments have greatly improved the presentation.

References

1. Andrew S. Glassner, editor. *An Introduction to Ray Tracing*. Academic Press, London, 1989.
2. David S. Immel, Michael F. Cohen, and Donald P. Greenberg. A radiosity method for non-diffuse environments. *Computer Graphics (Proc. ACM SIGGRAPH Conf.)*, **20**(4). pp. 133–142 (1986).
3. James T. Kajiya. The rendering equation. *Computer Graphics (Proc. ACM SIGGRAPH Conf.)*, **20**(4). pp. 143–150 (1986).
4. François X. Sillion, James R. Arvo, Stephen H. Westin, and Donald P. Greenberg. A global illumination solution for general reflectance distributions. *Computer Graphics (Proc. ACM SIGGRAPH Conf.)*, **25**(4). pp. 187–196 (1991).
5. John R. Wallace, Michael F. Cohen, and Donald P. Greenberg. A two-pass solution to the rendering equation: a synthesis of ray tracing and radiosity methods. *Computer Graphics (Proc. ACM SIGGRAPH Conf.)*, **21**(4). pp. 311–320 (1987).
6. Turner Whitted. An improved illumination model for shaded display. *Communications of the ACM*, **23**(6). pp. 343–349 (1980).
7. Paul S. Heckbert and Pat Hanrahan. Beam tracing polygonal objects. *Computer Graphics (Proc. ACM SIGGRAPH Conf.)*, **18**(3). pp. 119–127 (1984).
8. David Thomas, Arun N. Netravali, and D. S. Fox. Antialiased ray tracing with covers. *Comput. Graph. Forum*, **8**(4). pp. 325–336 (1989).
9. Masataka Ohta and Mamoru Maekawa. Ray-bound tracing for perfect and efficient anti-aliasing. *The Visual Computer*, **6**(3). pp. 125–133 (1990).
10. Robert L. Cook. Stochastic sampling in computer graphics. *ACM Transactions on Graphics*, **5**(1). pp. 51–72 (1986).
11. John Amanatides. Ray tracing with cones. *Computer Graphics (Proc. ACM SIGGRAPH Conf.)*, **18**(3). pp. 129–135 (1984).
12. Timothy L. Kay and James T. Kajiya. Ray tracing complex scenes. *Computer Graphics (Proc. ACM SIGGRAPH Conf.)*, **20**(4). pp. 269–278 (1986).
13. John M. Snyder and Alan H. Barr. Ray tracing complex models containing surface tessellations. *Computer Graphics (Proc. ACM SIGGRAPH Conf.)*, **21**(4). pp. 119–128 (1987).
14. Jon Genetti and Dan Gordon. Ray tracing with adaptive supersampling in object space. In N. Jaffe, editor, *Graphics Interface '93*, pp. 70–77 (1993).
15. Jon Genetti. Cone-object intersections for adaptive supersampling in object space. Technical Report TR93–018, Dept. of Computer Science, Texas A&M University (March 1993).
16. Jon Genetti. Image Synthesis with adaptive cone tracing, PhD Dissertation, Dept. of Computer Science, Texas A&M University (August 1993).
17. Robert L. Cook, Thomas Porter, and Loren Carpenter. Distributed ray tracing. *Computer Graphics (Proc. ACM SIGGRAPH Conf.)*, **18**(3). pp. 137–145 (1984).
18. Mark A. Z. Dippé and Erling Henry Wold. Antialiasing through stochastic sampling. *Computer Graphics (Proc. ACM SIGGRAPH Conf.)*, **19**(3). pp. 69–78 (1985).
19. Don P. Mitchell. Generating antialiased images at low sampling densities. *Computer Graphics (Proc. ACM SIGGRAPH Conf.)*, **21**(4). pp. 65–72 (1987).
20. James D. Foley, Andries van Dam, Steven K. Feiner, and John Hughes. *Computer Graphics:*

Principles and Practice. Addison-Wesley, Reading, Mass., 2nd edition (1990).

21. Don P. Mitchell. The antialiasing problem in ray tracing. In *SIGGRAPH '90 Course Notes*, volume 24, New York (August 1990). ACM.
22. John I. Yellot, Jr. Spectral consequences of photoreceptor sampling in the rhesus retina. *Science*, **221**. pp. 382–385 (1983).
23. Mark E. Lee, Richard A. Redner, and Samuel P. Uselton. Statistically optimized sampling for distributed ray tracing. *Computer Graphics (Proc. ACM SIGGRAPH Conf.)*, **19**(3). pp. 61–65 (1985).
24. James Painter and Kenneth Sloan. Antialiased ray tracing by adaptive progressive refinement. *Computer Graphics (Proc. ACM SIGGRAPH Conf.)*, **23**(3). pp. 281–288 (1989).
25. Kevin Weiler and Peter Atherton. Hidden surface removal using polygon area sorting. *Computer Graphics (Proc. ACM SIGGRAPH Conf.)*, **11**(2). pp. 214–222 (1977).
26. Mikio Shinya, Tokiichiro Takahashi, and Seiichiro Naito. Principles and applications of pencil tracing. *Computer Graphics (Proc. ACM SIGGRAPH Conf.)*, **21**(4). pp. 45–54 (1987).
27. Xiao D. He, Kenneth E. Torrance, François X. Sillion, and Donald P. Greenberg. A comprehensive physical model for light reflection. *Computer Graphics (Proc. ACM SIGGRAPH Conf.)*, **25**(4). pp. 175–186 (1991).
28. Paul S. Heckbert. Adaptive radiosity textures for bidirectional ray tracing. *Computer Graphics (Proc. ACM SIGGRAPH Conf.)*, **24**(4). pp. 145–154 (1990).
29. Eugene Fiume. Coverage masks and convolution tables for fast area sampling. *CVGIP: Graphical Models and Image Processing*, **53**(1). pp. 25–30 (1991).